Viscous Effects in Tube Flow Initiated by an Expansion Wave

Kwok-On Tong* and David A. Russell†
University of Washington, Seattle, Wash.

An examination is made of the effect of the turbulent boundary layer on the uniformity of the flow initiated by a nonsteady expansion wave traveling in a long, constant-area tube. Closed-form expressions for the flow perturbations first are obtained from the linearized equations of motion. Measured static pressure histories for both low- and high-tube Mach numbers are used for comparison. Detailed discussions of the limitations of the linearized model and its extension to high-tube Mach numbers are given. Agreement is shown between a modified version of the linearized model and the experimental results. A model of viscous nonsteady pipe flow is used to explain the nonlinear pressure decay observed at very large length-to-diameter ratios.

I. Introduction

AERODYNAMIC testing using the flow behind a nonsteady expansion wave traveling in a tube was proposed formally by Ludwieg.[1] Many small facilities subsequently were constructed based on this concept, and a number of studies were initiated on the use of large facilities for full-flight Reynolds number simulation.[2,3] It generally is believed that such "Ludwieg tubes" produce very high quality gas flow. The degree to which this is true is the subject of the present paper.

A major source of flow perturbation is the turbulent boundary layer behind the expansion wave. Mirels[4] and Becker[5] analyzed this boundary layer using 1/7th-power-law velocity profiles, while Starr and Scheuler[6] and Russell et al.[7] studied the layer experimentally. Becker[5] went on to consider its effect on the uniformity of the core flow, but his results are restricted to the origin of the expansion wave and to low-flow Mach numbers. As part of a general study of high performance Ludwieg tubes, Russell and Tong[8] stated simple new prediction formulas that also were restricted to the open end and to low Mach number. These had been developed from a linearized analysis based on modification of the core flow continuity equation to include the effect of the boundary-layer displacement thickness. The method was essentially that used by Demyanov[9] and Spence and Woods[10] for the flow behind a moving shock but with the shock now replaced by a zero-thickness expansion wave. Measurements of static pressure perturbation history at the open end of various tubes showed, surprisingly enough, that the predictions were applicable to high Mach number flow.

The question of viscous effects on tube flow initiated by an expansion wave is taken up more thoroughly in the present paper. The linearized prediction relations are developed formally for arbitrary Mach number in Sec. II. The procedure has a rigorous base,[11] and directly yields closed-form solutions for perturbations of the core flow at any position and time when power-law layers are used. In the latter respect, it is more convenient to use than the work of Mirels and Braun.[12] Although here restricted to the prediction of viscous induced perturbations, the approach also has application to the effects of initial pipe area and temperature nonuniformity.[8,13] Section III discusses static pressure histories taken at the open end of various tubes, extending the earlier work[8] to very large length-to-diameter ratios. Discrepancies arise between these measurements and the theory of Sec. II. These and other questions are resolved in Sec. IV, which successively considers the effects of boundary-layer model, finite-thickness expansion waves, boundary-layer growth within the exit nozzle, and merged boundary layers.

Received March 10, 1977; revision received Aug. 1, 1977.
Index categories: Nozzle and Channel Flow; Nonsteady Aerodynamics; Jets, Wakes, and Viscid-Inviscid Flow Interactions.

*Graduate Student, Department of Aeronautics and Astronautics; presently Senior Scientist, Avco Everett Research Laboratory, Inc. Member AIAA.
†Professor and Chairman, Department of Aeronautics and Astronautics. Associate Fellow AIAA.

II. Small Perturbation Analysis

Governing Equations

Figure 1 depicts a pressurized tube of length L and diameter D, in which flow has been initiated by the sudden removal of a diaphragm located at $x=0$. The expansion wave strength is controlled by a nearby choke, here shown schematically as the throat of a convergent-divergent nozzle. The flow leaving the tube ideally does not change until the head of the expansion wave has reflected off the closed end and arrived back at the nozzle. This test time is calculated readily (e.g., Refs. 2 and 14), as are the relations between the ideal flow behind the expansion wave (region 3) and the initial gas charge conditions in front of it (region 4). The present paper is concerned with viscous-induced perturbations of the gas behind the expansion wave from its ideal state.

The nonsteady continuity equation for the flow may be written in cylindrical coordinates as

$$\frac{\partial \rho}{\partial t} + \frac{\partial}{\partial x}(\rho u) + \frac{1}{r}\frac{\partial}{\partial r}(\rho v r) = 0$$

where ρ is the density, and u and v are the velocity components in the x and r directions, respectively. Multiplying by

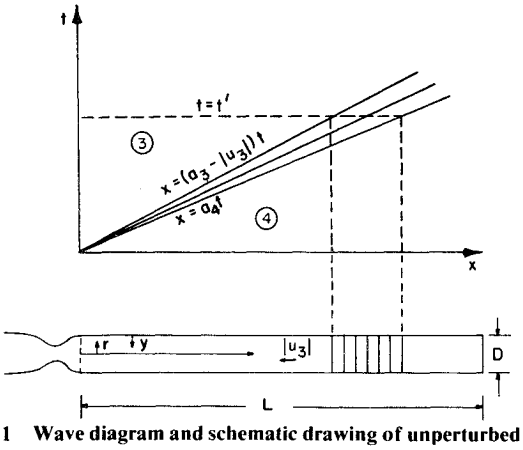

Fig. 1 Wave diagram and schematic drawing of unperturbed low.

r and integrating with respect to r from the tube centerline ($r=0$) to the wall at $r=D/2$ yields

$$\frac{\partial \rho_e}{\partial t}+\frac{\partial}{\partial x}(\rho_e u_e)\approx\frac{4}{D}\left[\frac{\partial}{\partial t}\int_0^\delta(\rho_e-\rho)\,dy+\frac{\partial}{\partial x}\int_0^\delta(\rho_e u_e-\rho u)\,dy\right] \tag{1}$$

where y is measured out from the wall (see Fig. 1). The subscript e denotes the condition of the gas external to the boundary layer, and δ is the boundary-layer thickness. Terms of $O(\delta/D)^2$ have been neglected, and it has been assumed that the gas outside of δ is independent of r, i.e., that $L/D\gg 1$. The corresponding momentum equation for the flow outside of δ is

$$\rho_e\left(\frac{\partial u_e}{\partial t}+u_e\frac{\partial u_e}{\partial x}\right)+\frac{\partial p_e}{\partial x}=0 \tag{2}$$

where p is the static pressure. Finally, as the expansion wave is an isentropic process, the entropy of each gas particle outside of δ remains constant. Thus, for a perfect gas,

$$\left(\frac{\partial}{\partial t}+u_e\frac{\partial}{\partial x}\right)\ln\frac{p_e}{\rho_e{}^\gamma}=0 \tag{3}$$

γ being the ratio of specific heats.

Using Eq. (3) to remove the ρ-derivatives in Eq. (1) yields

$$\frac{1}{a_e{}^2}\left(\frac{\partial p_e}{\partial t}+u_e\frac{\partial p_e}{\partial x}\right)+\rho_e\frac{\partial u_e}{\partial x}\approx\frac{4}{D}\cdot\left[\frac{\partial}{\partial t}\int_0^\delta(\rho_e-\rho)\,dy+\frac{\partial}{\partial x}\int_0^\delta(\rho_e u_e-\rho u)\,dy\right] \tag{4}$$

where a is the speed of sound. For simplicity, the expansion wave is treated as an isentropic zero-thickness wave traveling at a characteristic speed U_0. Following Becker's approach, the displacement thickness δ^* of the boundary layer behind this "expansion shock" then can be approximated by[13]

$$\frac{\delta^*}{D}\equiv\int_0^\delta\left(1-\frac{\rho u}{\rho_e u_e}\right)\frac{dy}{D}=\frac{1}{4}(1+m)K(Re_D)_3{}^{-m/(1+m)}\cdot\left(\frac{U_0t-x}{D}\right)^{1/(1+m)} \tag{5a}$$

where m is the power of the Reynolds number in the skin-friction law, K is a coefficient, $(Re_D)_3$ is the Reynolds number based on D and conditions in region 3, and U_0t-x is the distance behind the wave. Selection of a specific velocity profile power law determines m, while an additional assumption for the density distribution gives an expression for K.[13] For 1/7th-power-law profiles and constant ρ across the boundary layer, Becker's work[5] yields

$$m=1/4;\quad K^{5/4}=0.0715\frac{|u_3|}{U_0}\left(1+\frac{7}{9}\frac{|u_3|}{U_0}\right)^{-1} \tag{5b}$$

Combining Eqs. (4) and (5a),

$$\frac{1}{a_e{}^2}\left(\frac{\partial p_e}{\partial t}+u_e\frac{\partial p_e}{\partial x}\right)+\rho_e\frac{\partial u_e}{\partial x}\approx-(1+m)K(Re_D)_3{}^{-m/(1+m)}\cdot\frac{\partial}{\partial(U_0t-x)}\left[\rho_e u_e\left(\frac{U_0t-x}{D}\right)^{1/(1+m)}\right] \tag{6}$$

Linearization and Solution

If the flow outside δ is perturbed only slightly from the ideal condition of region 3, the $u_e(x,t)=-|u_3|+u'(x,t)$, $p_e(x,t)=p_3+p'(x,t)$, etc., and Eqs. (2) and (6) can be linearized to yield

$$\frac{1}{\rho_3 a_3{}^2|u_3|}\left(U_0\frac{\partial p'}{\partial\bar t}-|u_3|\frac{\partial p'}{\partial\bar x}\right)+\frac{1}{|u_3|}\frac{\partial u'}{\partial\bar x}\approx K(Re_D)_3{}^{-m/(1+m)}(\bar t-\bar x)^{-m/(1+m)} \tag{7a}$$

$$U_0\frac{\partial u'}{\partial\bar t}-|u_3|\frac{\partial u'}{\partial\bar x}+\frac{1}{\rho_3}\frac{\partial p'}{\partial\bar x}\approx 0 \tag{7b}$$

where the primed quantities are the perturbations and

$$\bar t\equiv U_0t/D,\quad \bar x\equiv x/D$$

Equations (7) govern the flow outside of δ. The viscous effects have appeared through the source term on the right-hand side of the continuity equation. This term contributes an effective tube diameter dependence on x and t through the displacement effect of the boundary layer.

Equations (7) are a hyperbolic system.[15] Choosing characteristic variables as

$$\eta\equiv\bar t-\frac{U_0/a_3}{M_0+1}(\bar t-\bar x)$$

$$\zeta\equiv\bar t-\frac{U_0/a_3}{M_0-1}(\bar t-\bar x)$$

with

$$M_0\equiv\frac{U_0}{a_3}+M_3;\qquad M_3\equiv|u_3|/a_3$$

they can be rewritten, algebraically combined, and integrated directly to yield

$$\frac{1}{\gamma M_3}\frac{p'}{p_3}=(1+m)K(Re_D)_3{}^{-m/(1+m)}\cdot\frac{M_0}{M_0{}^2-1}(\bar t-\bar x)^{1/(1+m)}+f(\zeta)-g(\eta) \tag{8a}$$

$$\frac{u'}{|u_3|}=(1+m)K(Re_D)_3{}^{-m/(1+m)}\cdot\frac{1}{M_0{}^2-1}(\bar t-\bar x)^{1/(1+m)}+f(\zeta)+g(\eta) \tag{8b}$$

Here $f(\zeta)$ and $g(\eta)$ are functions arising from the integration process, to be found by applying boundary conditions at the ends of the gas column. Note that the $\zeta=0$ characteristic represents the unperturbed tail of the expansion wave behind which [i.e., $0\le x\le(a_3-|u_3|)t$] ζ is negative.

Application of the Boundary Conditions

Equations (8) intimately involve the fictional speed U_0. This may be defined conveniently by writing mass continuity in a wave-fixed frame:

$$U_0\rho_4\equiv(U_0+|u_3|)\rho_3$$

Regions 3 and 4 are related isentropically through the Riemann invariant, and it follows that

$$U_0=\frac{M_3a_3}{\{1+[(\gamma-1)/2]M_3\}^{2/(\gamma-1)}-1} \tag{9}$$

a velocity between a_4 and $a_3-|u_3|$ (see Fig. 1). Allowing perturbations from conditions 3, a more general expansion

shock velocity is given by

$$U(\bar{t})\rho_4 = [U(\bar{t}) - u_e(\bar{t})]\rho_e(\bar{t})$$

This may be differentiated and rewritten for small perturbations of an ideal gas as

$$u' \approx U'\left[1 - \frac{p_4}{p_3}\left(\frac{a_3}{a_4}\right)^2\right] + U_0\left[\frac{p_4}{p_3}\left(\frac{a_3}{a_4}\right)^2\frac{p'}{p_3} - 2\frac{p_4}{p_3}\left(\frac{a_3}{a_4}\right)\frac{a'}{a_4}\right]$$

Relating u', a', and p' through the Riemann invariant and the condition of isentropic flow, there is obtained

$$\frac{p'}{\gamma M_3 p_3}, \quad \frac{u'}{|u_3|} = \frac{U'/U_0}{[U_0/a_3(a_4/a_3)^{2/(\gamma-1)} - 1]} \tag{10}$$

for the flow perturbations immediately behind the wave. For small perturbations, these boundary conditions may be applied along the unperturbed expansion shock path $x = U_0 t$. Comparing Eqs. (8) at $\bar{x} = \bar{t}$ with Eqs. (10) then yields

$$f(\bar{t}) = \frac{U'(\bar{t})\,U_0}{[U_0/a_3(a_4/a_3)^{2/(\gamma-1)} - 1]}; \quad g(\bar{t}) = 0$$

Since g is a function of η only, the condition that $g = 0$ along $\bar{x} = \bar{t}$ leads to the conclusion that

$$g(\eta) = 0 \tag{11}$$

everywhere behind the expansion shock.

A boundary condition at the nozzle inlet ($\bar{x} = 0$) is needed in order to determine $f(\zeta)$. For $L/D \gg 1$, the nozzle is much shorter than the tube, and one-dimensional steady flow relations can be applied between the nozzle throat and the tube exit. If the throat is choked, and if its boundary-layer thickness-to-diameter ratio can be neglected compared to that at the nozzle inlet, then the relative change of core cross-sectional area at the inlet is

$$\frac{dA}{A} \approx -4\frac{\delta^*}{D}\bigg|_{\bar{x}=0} \approx -\frac{(1-M_3^2)}{1+[(\gamma-1)/2]M_3^2}\frac{M'}{M_3}\bigg|_{\bar{x}=0} \tag{12}$$

for $\delta^*/D|_{\bar{x}=0} \ll 1$. Since

$$\frac{M'}{M_3} \approx -\left(\frac{u'}{|u_3|} + \frac{\gamma-1}{2\gamma}\frac{p'}{p_3}\right)$$

Eqs. (8) at $\bar{x} = 0$, together with Eqs. (5a) and (11), may be used with Eq. (12) to yield

$$f(\zeta) = -(1+m)K(Re_D)_3^{-m/(1+m)}\left(\frac{M_0-1}{M_3-1}\zeta\right)^{1/(1+m)} \cdot \frac{\{1+[(\gamma-1)/2]M_3^2\}(M_0^2-1) + (1-M_3^2)\{1+[(\gamma-1)/2]M_3M_0\}}{\{1+[(\gamma-1)/2]M_3\}(M_0^2-1)(1-M_3^2)} \tag{13}$$

Linearized Theory Predictions

Equations (11) and (13) may be used with Eq. (8) to calculate p' and u' at any point in the flow. Figure 2 shows the normalized pressure perturbation for $\gamma = 1.4$ and various values of M_3. U_0 was obtained from Eq. (9), and m and k from Eqs. (5b). The ordinate grouping collects a weak dependence on $(Re_D)_3$ and an almost linear dependence on $\bar{t}$. The abscissa is the fractional distance from the nozzle inlet ($\bar{x}/\bar{t} = 0$) to the expansion shock position ($\bar{x}/\bar{t} = 1$) at the same instant of time. The position of the unperturbed tail of the expansion wave (see Fig. 1) can be written in the form $\bar{x}/\bar{t} = (1-M_3)/(M_0-M_3)$. Predictions for the region between this and the expansion shock are of questionable validity and are not shown on the figure. The curves exhibit a positive perturbation near the expansion wave, falling to a negative perturbation at the nozzle inlet. The former occurs because a positive $p'(t)$ caused by the constriction effect of

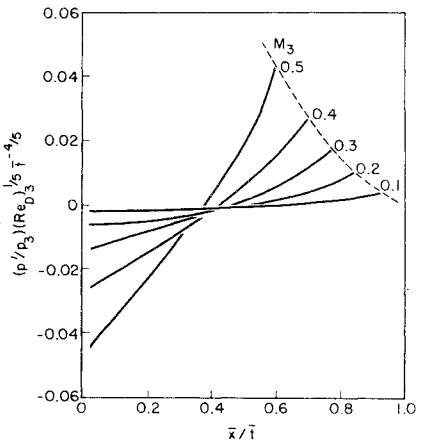

Fig. 2 Pressure perturbation in tube flow initiated by a centered nonsteady expansion wave at $\bar{x}$, $\bar{t} = 0$ [Eqs. (8, 11, and 13); constant density 1/7th-power-law boundary layer with U_0 given by Eq. (9); $\gamma = 1.4$].

the growing δ^* continuously weakens the expansion wave and the expansion shock representing it. However, the nozzle inlet boundary condition requires that M increase as δ^* at $\bar{x} = 0$ grows. Therefore, secondary expansion waves are sent back from the inlet, and p' at $\bar{x}/\bar{t} = 0$ is negative. These effects all are seen to become more severe as M_3 is increased.

The velocity perturbation curves are of similar shape to those in Fig. 2 but have a nozzle inlet magnitude that can exceed p'/p_3 by over an order of magnitude at low M_3. Once p' and u' have been determined, the perturbations in temperature, speed of sound, Mach number, stagnation temperature, and stagnation pressure can be found through the following relations:

$$T'/T_3 = [(\gamma-1)/\gamma]p'/p_3 \tag{14a}$$

$$a'/a_3 = \tfrac{1}{2}T'/T_3 \tag{14b}$$

$$M'/M_3 = -(u'/|u_3| + a'/a_3) \tag{14c}$$

$$T_0'/T_{0_3} = [(\gamma-1)M_3^2/\{1+[(\gamma-1)/2]M_3^2\}] \cdot M'/M_3 + T'/T_3 \tag{14d}$$

$$p_0'/p_{0_3} = [\gamma/(\gamma-1)]T_0'/T_{0_3} \tag{14e}$$

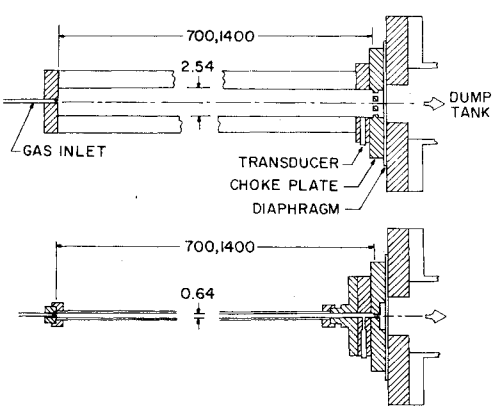

Fig. 3 Scale drawing of experimental setup (dimensions in centimeters).

For $M_3 \ll 1$, Eqs. (8, 9, 11, and 13) simplify to

$$\frac{p'}{p_3} \approx (1+m)K(Re_D)_3^{-m/(1+m)} \frac{2\gamma}{\gamma+1}\left\{\left(1+\frac{\gamma+1}{8}M_3\right)\times\left(\bar{t}-\bar{x}\right)^{1/(1+m)} - \left[\bar{t}-\left(1+\frac{\gamma+1}{4}M_3\right)\bar{x}\right]^{1/(1+m)} \times\left(1+\frac{3}{8}(\gamma+1)M_3\right)\right\} \quad (15a)$$

$$\frac{u'}{|u_3|} \approx (1+m)K(Re_D)_3^{-m/(1+m)} \frac{2}{\gamma+1}\frac{1}{M_3} \times\left\{\left(1-\frac{\gamma+1}{8}M_3\right)(\bar{t}-\bar{x})^{1/(1+m)} - \left[\bar{t}-\left(1+\frac{\gamma+1}{4}M_3\right)\bar{x}\right]^{1/(1+m)}\left(1+\frac{3}{8}(\gamma+1)M_3\right)\right\} \quad (15b)$$

which for $\bar{x}=0$ reduce to those reported previously.[8] Regardless of the value of M_3, the maximum nozzle inlet perturbation will occur at the end of the test time. With the expansion wave replaced by an expansion shock, this time is determined by the arrival at $\bar{x}=0$ of the η characteristic that originates when the shock strikes the closed end. It is given by

$$\bar{t} = (M_0+1)/(1+M_3)L/D \quad (16)$$

III. Experimental Studies

Equipment and Procedure

The static pressure time history was measured just upstream of the nozzle inlet end of various supply tubes for a range of operating conditions. The tubes were assembled from nominal 7-m lengths of 2.5-cm-i.d. cold-rolled steel pipe with a 1.6-cm wall, or 0.64-cm-i.d. 304 stainless high-pressure tubing with a 0.17-cm wall. As indicated on Fig. 3, two lengths of each tube were available, providing actual L/D values of 280, 540, 1100, and 2200. M_3 was selected through use of a choke plate involving one or more orifices for all except the large D runs at $M_3 > 0.6$. The diaphragm itself served as the choke in the latter cases, M_3 being calculated from the measured values of p_4 and p_3 (see below). A quartz pressure transducer (Kistler model 603A) was located just upstream of the choke, while a prescribed soft Al diaphragm was located downstream.

Bottled N_2 was admitted through an orifice at the opposite end of the tube. The orifice diameter of 0.08 cm for the 2.5-cm tube and 0.04 cm for the 0.64-cm tube provided essentially closed ends. Upon pressure bursting, the four diaphragm petals opened into a square-hole receiving plate, and the gas exhausted into a 4-m^3 tank. The 50-100-atm pressure level at diaphragm rupture was recorded on a maximum-pressure-indicating Bourdon-tube gage that was connected to the gas inlet. The output of the pressure transducer at the open end was fed to a preamplifier and thence to a single-sweep oscilloscope that was triggered by an accelerometer mounted on the diaphragm receiving flange. The sensitivity and linearity of the gage output were checked by static calibrations.

p_3 was determined from the calculated M_3 and measured p_4, except for the large D, $M_3 > 0.6$ runs, where it was read directly from the oscilloscope trace. Pressure changes then could be expressed as a percentage of p_3, as on Fig. 4. Here, the left-hand oscilloscope trace is for low M_3 and L/D. The expansion wave is seen to clear the gage in the first millisecond of run time, dropping the pressure to p_3. The expanded vertical scale of the trace shows a subsequent decline in p until the expansion wave head returns from the end of the tube.

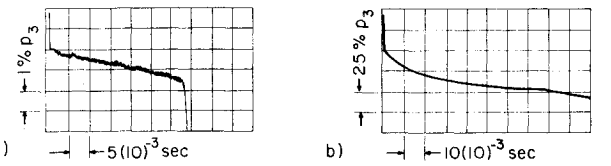

Fig. 4 Static pressure perturbation at open end of tube: a) $M_3 = 0.1$, $L/D = 280$, $D = 2.5$ cm, $p_4 = 60$ atm; b) $M_3 = 0.8$, $L/D = 2200$, $D = 0.64$ cm, $p_4 = 60$ atm (N_2 at $T_4 = 300$ K).

The absolute value of the pressure drop is small compared to that observed for the high M_3, high L/D example of Fig. 4b. The decay process also has become distinctly nonlinear in the latter case. Furthermore, the return of the reflected head of the expansion wave is now just discernible as a slight change of slope at $80(10)^{-3}$ sec, delayed $10(10)^{-3}$ sec from the ideal value for this case. Traces at conditions intermediate to Figs. 4a and 4b show that increases in M_3 and/or L/D lead to larger values of p'/p_3, increased nonlinearity of the decay, and obscuration of the end of the run time.

The measurement of small values of p'/p_3 raises the question of extraneous effects. No special care was taken with the interior of the tubes, as the operating conditions were such that turbulent boundary layers were expected within ≈ 10 cm of the expansion wave. However, it has been stated[8] that the contribution of cross-sectional area and axial temperature nonuniformities to $p'/p_3|_{\bar{x}=0}$ increases approximately linearly with M_3 to give perturbations of the order of the nonuniformity at $M_3 = 1$. Thus, keeping these nonuniformities to $< 1\%$ should restrict their contribution to lower order for $p'/p_3|_{\bar{x}=0}$ values exceeding 0.1 M_3. Satisfactory cross-sectional tolerances were expected from the manufacturing processes and were checked by diameter measurements at the tube ends. On the other hand, measurements with thin-film heat-transfer gages directed that tube charging be carried out over intervals of several minutes in order to avoid significant axial temperature variation due to compression heating.

Data Correlation

Figure 5 collects p'/p_3 read from the oscilloscope traces at the time when the return of the reflected head of the expansion wave is indicated. It has been plotted against calculated M_3 for the four different values of L/D. Each symbol represents at least five separate runs, the extreme values from each set being contained within the symbol size on the figure unless otherwise indicated by the additional attached bars. The p_4 range proved to be too small to be able to separate out pressure level trends. As expected, p'/p_3 is seen to be strongly dependent on M_3 and L/D, climbing from 1% to over 50% for the extreme cases. Additional single runs at $M_3 \approx 0.7$ and ≈ 1.0 were supportive of the trends seen on the figure.

The p'/p_3 that went into Fig. 5 have been multiplied by their individual values of $(p_4D)^{1/5}$ $(L/D)^{-4/5}$ and replotted vs M_3 on Fig. 6. The grouping comes naturally from Eqs. (8, 11, and 13), with $\bar{t}$ given by Eq. (16) and $m = 1/4$, equivalent to the assumption of a 1/7th-power-law boundary layer [Eqs. (5b)]. The p_4D term carries the Reynolds number dependence, while L/D brings in the length dependence at the end of the run time. Figure 6 shows that use of this multiplicative factor goes a long way toward correlating the data, perhaps overcorrecting it for the large L/D cases at moderate-to-large M_3. The predictions of Eqs. (8, 11, and 13) also are shown, here evaluated for $T_4 = 300$ K nitrogen. Again Eqs. (5b) were used, with U_0 given by Eq. (9) and $\bar{t}$ by Eq. (16). The agreement at low M_3 is seen to be excellent, and the essentially linear decay of Fig. 4a is close to the predicted $t^{-4/5}$ dependency. The analysis predicts a similar decay with a perturbation magnitude approaching infinity as M_3 approaches 1, trends that clearly are not borne out by the experiments.

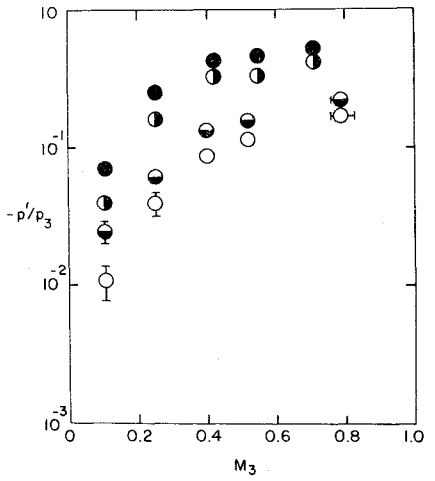

Fig. 5 Maximum measured pressure perturbation (N_2 at $T_4 = 300$ K, $p_4 = 50$-100 atm; ○: $L/D = 280$, $D = 2.5$ cm; ◒: $L/D = 540$, $D = 2.5$ cm; ◒: $L/D = 1100$, $D = 0.64$ cm; ●: $L/D = 2200$, $D = 0.64$ cm).

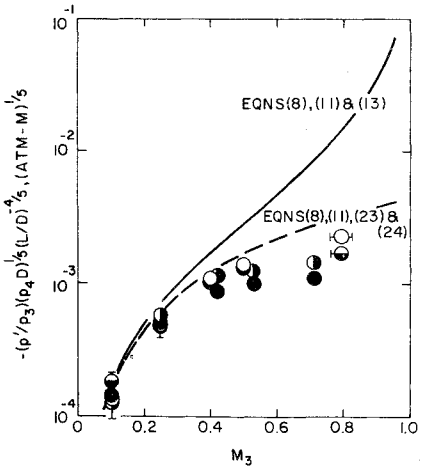

Fig. 6 Comparison of experimental data with prediction [data symbols as on Fig. 5; solid line is small perturbation analysis; dashed line is improved small perturbation analysis incorporating nozzle boundary layer given by Eq. (24) with $H_{12} = 72/56$].

IV. Discussion

Boundary-Layer Model

The analysis of Sec. II can only be as good as the boundary-layer input. Equations (5b) were generalized to arbitrary power law using shear stress information given by Kutateladze and Leont'ev.[16] Calculations then showed that changing from a 1/7th to a 1/10th power law reduces p'/p_3 by at most 10%, as does evaluation of U_0 based on boundary-layer matching considerations.[5] Relaxation of the constant-density approximation in the boundary-layer model[5,13] gives a δ^* reduction that reaches 30-40% at high M_3, with an approximately equivalent reduction in p'/p_3 [see Eqs. (5a, 8, and 13)], whereas a different model by Mirels[4] gives a 30-40% increase. Recent experimental results by Russell et al.[7] indicate an actual δ^* following the present approximate model between the more complete theories. Even ignoring these experiments, Fig. 6 shows an overprediction by the linearized analysis at high M_3 which is too extreme to be accounted for by uncertainties in δ^* alone.

Expansion Wave Boundary Condition

The boundary conditions that were applied (Sec. II) thus must be reconsidered at high M_3. The expansion wave now spreads out, and treatment as a discontinuity with a zero-pressure-gradient boundary layer growing behind it becomes questionable. The flow in the wave is inherently nonsteady; however, it is convenient to define a dimensionless distance at fixed time between any point x and the head of the expansion wave:

$$\psi \equiv 1 - x/(a_4 t)$$

The unperturbed properties of the flow remain constant along each $\psi = \text{const}$ line in a centered expansion wave. With subscript i referring to this unperturbed flow, the Riemann invariant, together with the definition of the wave slope in the x-t plane, leads to

$$a_i = a_4\{1 - [(\gamma-1)/(\gamma+1)]\psi\} \tag{17a}$$

$$u_i = -a_4[2/(\gamma+1)]\psi \tag{17b}$$

and similar relations for the other unperturbed quantities in the isentropic flow. Furthermore, the boundary-layer thickness δ is given in the literature[5] as

$$\delta/D \approx 0.11(Re_D)_4^{-1/5}(a_4 t/D)^{4/5}\psi^{7/5} \tag{18}$$

for 1/7th-power velocity and density-change profiles. $(Re_D)_4$ is the Reynolds number based on D and the speed of sound and kinematic viscosity in the charge gas. With wall temperature equal to T_4, Eqs. (2, 4, and 18) can be linearized to yield

$$a_4\frac{\partial u'}{\partial \bar{t}} + u_i\frac{\partial u'}{\partial \bar{x}} + u'\frac{\partial u_i}{\partial \bar{x}} + \frac{1}{\rho_i}\frac{\partial p'}{\partial \bar{x}} - \frac{p'}{\rho_i^2 a_i^2}\frac{\partial p_i}{\partial \bar{x}} = 0 \tag{19a}$$

$$\frac{1}{\rho_i a_i^2 |u_i|}\left(a_4\frac{\partial p'}{\partial \bar{t}} + u_i\frac{\partial p'}{\partial \bar{x}} + u'\frac{\partial p_i}{\partial \bar{x}}\right) + \frac{1}{|u_i|}\frac{\partial u'}{\partial \bar{x}} + \frac{\gamma p'}{\rho_i a_i^2 |u_i|}\frac{\partial u_i}{\partial \bar{x}}$$

$$= 0.11(Re_D)_4^{-1/5}\bar{t}^{-1/5}\psi^{7/5}\left[0.29 + \psi^{-1}\left(1-\frac{\psi}{6}\right)^{-1} \times (1.68 - 1.03\psi + 0.09\psi^2)\right] \tag{19b}$$

where terms of order $(\delta/D)^2$ and higher again have been ignored, the equation for the unperturbed flow has been subtracted out, and the dimensionless independent variables now are defined as

$$\bar{t} \equiv a_4 t/D, \quad \bar{x} \equiv x/D$$

Equations (19) form a system of hyperbolic partial differential equations[15] similar to Eqs. (7). They are quasilinear with coefficients that are known functions of $\bar{x}$ and $\bar{t}$ and characteristic directions given by $(-a_i + u_i)$ and $(a_i + u_i)$. The characteristic variables are chosen to be

$$\psi \equiv 1 - \bar{x}/\bar{t}$$

$$\omega \equiv \bar{t}[5/6 + \bar{x}/(6\bar{t})]^3$$

for $\gamma = 1.4$. In terms of these variables, Eqs. (19) can be rewritten as[13]

$$\frac{\partial \Lambda}{\partial \omega} + 0.667\frac{\Delta}{\omega} - 0.452(Re_D)_4^{-1/5}\omega^{4/5} \times \left(1-\frac{\psi}{6}\right)^{3/5}\psi^{7/5}(0.350 - 0.155\psi + 0.00803\psi^2) = 0 \tag{20a}$$

$$\frac{\partial \Delta}{\partial \psi} + \left(1-\frac{\psi}{6}\right)^{-1}\frac{\Delta}{2} + 0.276(Re_D)_4^{-1/5}\omega^{9/5} \times \left(1-\frac{\psi}{6}\right)^{-2/5}\psi^{7/5}(0.350-0.155\psi+0.00803\psi^2) = 0 \quad (20b)$$

where

$$\Lambda \equiv (1-\psi/6)^6 \bar{t} u'/a_4 + (\bar{t}/\gamma)p'/p_4$$

$$\Delta \equiv (1-\psi/6)^6 \bar{t} u'/a_4 - (\bar{t}/\gamma)p'/p_4$$

Equation (20b) can be integrated at constant ω to give

$$\Delta = -0.276(Re_D)_4^{-1/5}\omega^{9/5}(1-\psi/6)^3 \cdot \int (1-\psi/6)^{-17/5}\psi^{7/5}(0.350-0.155\psi+0.00803\psi^2)\,d\psi$$

where the boundary conditions that u' and p' are zero along the head of the expansion wave ($\psi = 0$) have been applied. The integral may be evaluated by expanding $(1-\psi/6)^{-17/5}$ in a binominal series. Equation (20a) then may be integrated, with the constant of integration set equal to zero so that u' and p' are everywhere zero at $t = 0$. Using Eqs. (17) and considerable algebra, the expressions for Δ and Λ yield

$$p'/p_i \approx 1.58(Re_D)_4^{-1/5}\bar{t}^{4/5}\psi^{7/5}(1-\psi/6)^{-1} [(1-\psi/6)^{12/5}(0.020\psi+0.002\psi^2)+0.039 - 0.017\psi+0.001\psi^2] \quad (21a)$$

$$u'/|u_i| \approx 1.36(Re_D)_4^{-1/5}\bar{t}^{4/5}\psi^{2/5}[(1-\psi/6)^{12/5} \times (-0.009\psi-0.001\psi^2)+0.039-0.017\psi+0.001\psi^2)] \quad (21b)$$

The perturbations of other properties in the core flow can be calculated through use of Eqs. (14).

The perturbations at the tail of expansion wave as based on the analyses of Sec. II (i.e., see Fig. 2) and this section have been compared for various M_3. The 1/7th-power-law boundary-layer model was used in both analyses. A factor of 2 reduction in u'/u_3 was predicted by the analysis in this section, with p'/p_3 reduced 30-40% over the full range of M_3. As the effect of nonzero wave thickness is expected to be a maximum at the tail of expansion wave, the differences are too small to account for the discrepancy between the predicted open-end pressure perturbation and experimental result at high M_3.

Nozzle Inlet Boundary Condition

The nozzle inlet boundary condition remains to be reconsidered. As M_3 approaches unity, the nozzle throat δ^* no longer can be neglected in determining the effective nozzle inlet-to-throat area ratio. For small δ^*/D, Eq. (12) is rewritten as

$$-4\frac{\delta^*}{D}\bigg|_{\bar{x}=0}\left[1-\frac{\delta^*}{D}\bigg|_t\Big/\frac{\delta^*}{D}\bigg|_{\bar{x}=0}\right] = -\frac{1-M_3^2}{1+[(\gamma-1)/2]M_3^2}\frac{M'}{M_3}\bigg|_{\bar{x}=0} \quad (22)$$

where $\delta^*/D|_t$ is the fractional boundary-layer displacement thickness at the nozzle throat. Following the procedure of Sec. II,

$$f(\zeta) = -(1+m)K(Re_D)_3^{-m/(1+m)}\left(\frac{M_0-1}{M_3-1}\zeta\right)^{1/(1+m)}\left\{\frac{\{1+[(\gamma-1)/2]M_3^2\}(M_0^2-1)+(1-M_3^2)\{1+[(\gamma-1)/2]M_3M_0\}}{\{1+[(\gamma-1)/2]M_3\}(M_0^2-1)(1-M_3^2)} - \left(\frac{\delta^*}{D}\bigg|_t\Big/\frac{\delta^*}{D}\bigg|_{\bar{x}=0}\right)\frac{1+[(\gamma-1)/2]M_3^2}{(1-M_3^2)\{1+[(\gamma-1)/2]M_3\}}\right\} \quad (23)$$

In general, $\delta^*/D|_t/\delta^*/D|_{\bar{x}=0}$ must be calculated for each inlet design, operating condition, and $\bar{t}$. However, the contribution of the wall shear stress between the inlet and the throat can be ignored when L/D and $\bar{t} \gg 1$. Integrating the steady axially symmetric momentum integral equation along the nozzle then gives

$$\frac{\delta^*}{D}\bigg|_t\Big/\frac{\delta^*}{D}\bigg|_{\bar{x}=0} = M_3^{(1+H_{12})}\left[\frac{1+[(\gamma-1)/2]M_3^2}{(\gamma+1)/2}\right]^{-(1+H_{12})/2} \quad (24)$$

where H_{12} is the ratio of the displacement thickness to the momentum thickness, here taken to be constant. With $H_{12} = 72/56$, corresponding to a steady incompressible 1/7th-power-law boundary layer, this equation, together with Eqs. (8, 11, and 23), gives the dashed line of Fig. 6. This prediction for the pressure perturbation is seen to be reduced significantly from the previous one at high M_3, with a considerably better agreement with experiment.

Steady integral calculations were carried out for the compressible turbulent boundary layer in a series of axisymmetric nozzles given by equal radius arcs tangent to the x direction and to each other at 45 deg. These gave values of $\delta^*/D|_t/\delta^*/D|_{\bar{x}=0}$ at high-to-moderate M_3 and $\bar{t} > 10$ which were some 30% larger than those estimated previously, suggesting even better agreement with the data on Fig. 6. Furthermore, the calculations showed that the bracketed quantity on the left-hand side of Eq. (22) has a magnitude within ±10% of the coefficient of M'/M_3 for any M_3 when $\bar{t} > 10$. Equation (22) thus may be approximated by

$$4\delta^*/D|_{\bar{x}=0} = M'/M_3|_{\bar{x}=0} \quad (25)$$

leading to

$$f(\zeta) = -(1+m)K(Re_D)_3^{-m/(1+m)}\left(\frac{M_0-1}{M_3-1}\zeta\right)^{1/(1+m)} \times \frac{M_0^2+[(\gamma-1)/2]M_3M_0}{(M_0^2-1)\{1+[(\gamma-1)/2]M_3\}} \quad (26)$$

Use of this equation reduces $-p'/p_3$ 20% from the dashed line on Fig. 6 at high M_3. The result is essentially the same as that given by Eqs. (15) evaluated at $\bar{x} = 0$, this being explained partially by the fact that Eq. (12) evaluated for small M_3 becomes identical to Eq. (25).

Merged Boundary Layers

The various boundary-layer models previously mentioned show that $\delta = D/2$ at a distance of some $100D$ behind the expansion wave. The flow in the nozzle region subsequently will become fully developed, and there is no need for the generation of secondary expansion waves at the nozzle inlet (Sec. II). Thus, for very large L/D, much of the flow can be characterized as a pipe flow with a length that increases with time. The momentum equation for a steady, fully developed pipe flow is

$$\frac{\partial}{\partial x}\left[p(1+\gamma M^2)\right] = \frac{1}{2D}\left[0.316(Re_D)_3^{-1/4}\right]\gamma p M^2$$

where the Blasius friction law has been used, and M is averaged over the cross section. Ignoring the weak dependence of the skin-friction coefficient on x and changes in expansion shock strength, this can be integrated from the

nozzle inlet ($x=0$) to the expansion shock ($x=U_0t$) to give

$$\frac{p}{p_3} \approx \exp\left[-0.16(Re_D)_3^{-1/4}\left(\frac{\overline{\gamma M^2}}{1+\gamma M^2}\right)\bar{t}\right] \tag{27}$$

where $\bar{t}$ is again $\equiv U_0t/D$, and its coefficient is averaged throughout the flow.

Small values of the coefficient of $\bar{t}$ in Eq. (27) lead to an approximately linear decay that turns out to be close to the predictions of Sec. II and the result of Fig. 4a. Furthermore, the nonlinear decay of Fig. 4b corresponds to large values of this coefficient and is predicted within a factor of 2 by Eq. (27) at high M_3 and large L/D. The generally reduced level and rate of pressure decay given by the present model explains why the L/D data of Fig. 6 tend to overcorrected by linearized theory scaling. More detailed study would require a model that allows for variations of M along the tube, a changing U_0, and proper inclusion of the nonsteady terms.

V. Conclusions

The spatial and temporal uniformity of the flow initiated in a long pressurized tube by suddenly opening one end has been studied both analytically and experimentally. A small perturbation theory using a zero-thickness expansion wave was developed [Eqs. (8, 11, and 13)] and found to be in excellent agreement with measured open-end pressure perturbation at low M_3 but to overpredict the pressure perturbation drastically as M_3 approaches one. The boundary-layer model, the speed assigned to the expansion shock, and the assumption of zero-thickness expansion wave were discussed and found to make relatively small contributions to the overprediction. Neglect of the effective exit throat boundary condition turns out to be the primary cause, and a modification to this boundary condition is proposed [Eqs. (23) and (24) to replace Eq. (13)]. The result is observed to apply to arbitrary M_3. Calculation of boundary-layer growth within a family of exit nozzles lead to a simplification of this boundary condition [Eq. (25)] and explanation of the high M_3 applicability of a low M_3 solution [Eq. (15)]. Finally, a model of viscous nonsteady pipe flow has been used to explain the observed nonlinear pressure decay and its overprediction by linearized theory at large L/D.

Acknowledgment

This study was supported by NASA under Grant Nos. NGL 48-001-057 and NGR 48-002-107.

References

[1] Ludwieg, H., "Der Rohrwindkanal," *Zeitschrift für Flugwisserschaften*, Vol. 3, July 1955, pp. 206-216.

[2] Enkenhus, K. R. and Merritt, D. L., "Evaluation of Two Types of Facilities to Fulfill the Need for High Reynolds Number Transonic Testing," Naval Ordnance Lab., White Oak, Silver Spring, Md., NOLTR 71-147, July 1971.

[3] Whitfield, J. D., Schueler, C. J., and Starr, R. F., "High Reynolds Number Transonic Wind Tunnels-Blowdown or Ludwieg Tube?," *Facilities and Techniques for Aerodynamic Testing at Transonic Speeds and High Reynolds Number*, AGARD-CP-83-71, 1971.

[4] Mirels, H., "Boundary Layer Behind Shock or Thin Expansion Waves Moving into Stationary Fluid," NACA TN 3712, 1956.

[5] Becker, E., "Reibungswirkungen beim Rohrwindkanal," Mitt. aus dem Max-Planck-Institut fuer Stroemungsforschung u.d. Aerodynamischen Versuchsanstalt, No. 20, 1958.

[6] Starr, R. F. and Schueler, C. J., "Experimental Studies of a Ludwieg Tube High Reynolds Number Transonic Tunnel," *AIAA Journal*, Vol. 12, March 1974, pp. 267-268.

[7] Russell, D. A., Knoke, G. S., and Wai, J. C., "Uniformity of Ludwieg Tube Flows," *Proceedings of the Xth International Shock Tube Symposium*, Kyoto, Japan, 1975, pp. 244-251.

[8] Russell, D. A. and Tong, K.-O., "Aerodynamics of High-Performance Ludwieg Tubes," *AIAA Journal*, Vol. 11, May 1973, pp. 642-648.

[9] Demyanov, Yu. A., "The Influence of the Boundary Layer on the Character of the Flow of Gas in a Tube Behind a Moving Shock Wave," *Prikladnaia Matematika i Mekhanika*, Vol. 21, No. 4, 1957, pp. 473-477; also R.A.E. Library Transl. 796, 1959.

[10] Spence, D. A. and Woods, B. A., "Boundary Layer and Combustion Effects in Shock Tube Flows," *Hypersonic Flow*, edited by A. D. Collar and J. Tinkler, Butterworths, London, 1960, pp. 153-180.

[11] Spence, D. A. and Woods, B. A., "A Review of Theoretical Treatments of Shock-Tube Attenuation," *Journal of Fluid Mechanics*, Vol. 19, June 1964, pp. 161-174.

[12] Mirels, H. and Braun, W. H., "Perturbed One-Dimensional Unsteady Flows Including Transverse Magnetic-Field Effects," *The Physics of Fluids*, Vol. 5, March 1962, pp. 259-265.

[13] Tong, K.-O., "On the Uniformity of the Flow Initiated by a Nonsteady Expansion Wave," Ph.D. Thesis, Univ. of Washington, Seattle, Wash., Aug. 1973.

[14] Cable, A. J. and Cox, R. N., "The Ludwieg Pressure Tube Supersonic Wind Tunnel," *Aeronautical Quarterly*, Vol. 14, Pt. 2, May 1963, pp. 143-157.

[15] Courant, R. and Friedrichs, K. O., *Supersonic Flow and Shock Waves*, Interscience, New York, 1948, pp. 37-45.

[16] Kutateladze, S. S. and Leont'ev, A. I., *Turbulent Boundary Layers in Compressible Gases*, Edward Arnold, London, 1964, pp. 33-38.